frontiers | Frontiers in Sustainable Food Systems

TYPE Original Research
PUBLISHED 17 November 2023
DOI 10.3389/fsufs.2023.1271921

OPEN ACCESS

EDITED BY
Yiming Zhang,
Zhejiang Agriculture and Forestry University, China

REVIEWED BY
Qinhe Pan,
Hainan University, China
Xiulan Sun,
Jiangnan University, China

*CORRESPONDENCE
Yansong Zhang
✉ nora_zhang@163.com
Shuangshou Wang
✉ wangss17@ahut.edu.cn

RECEIVED 03 August 2023
ACCEPTED 20 October 2023
PUBLISHED 17 November 2023

CITATION
Zhang Y, Ding Y, Ma Y, Zhang Z, Wang Y, Li D and Wang S (2023) High-capacity boronate affinity-based template-immobilized surface imprinted silica nanoparticles for rapid, selective, and efficient extraction and determination of lincomycin in milk and chicken.
Front. Sustain. Food Syst. 7:1271921.
doi: 10.3389/fsufs.2023.1271921

High-capacity boronate affinity-based template-immobilized surface imprinted silica nanoparticles for rapid, selective, and efficient extraction and determination of lincomycin in milk and chicken

Yansong Zhang[1]*, Yihan Ding[2], Yidan Ma[2], Zixin Zhang[2], Yipei Wang[2], Daojin Li[2] and Shuangshou Wang[3]*

[1]School of Food and Drug, Luoyang Normal University, Luoyang, China, [2]Henan Key Laboratory of Function-Oriented Porous Materials, College of Chemistry and Chemical Engineering, Luoyang Normal University, Luoyang, China, [3]School of Chemistry and Chemical Engineering, Anhui University of Technology, Ma'anshan, China

Background: Lincomycin, a natural antibiotic, is widely used by animal and fishery husbandries to prevent infections and treat diseases. It endangers people's health when they eat foods containing lincomycin residue, especially the frequent consumption of milk and chicken products containing lincomycin. Hence, it is extremely important to evaluate the content of lincomycin in food samples. However, a direct analysis of lincomycin in milk and chicken is quite difficult because of its very low concentration level and the presence of undesirable matrix effects. Therefore, selective and efficient extraction of lincomycin from complex food samples prior to its quantification is required.

Results: In this study, lincomycin-imprinted silica nanoparticles were prepared according to boronate affinity-based template-immobilized surface imprinting. Silica nanoparticles and boronic acid ligands 3-fluoro-4-formylphenylboronic acid were used as supporting materials and functional monomers, respectively. The prepared lincomycin-imprinted silica nanoparticles exhibited several significant results, such as good specificity, high binding capacity (19.45 mg/g), fast kinetics (6 min), and low binding pH (pH 5.0) toward lincomycin. The reproducibility of lincomycin-imprinted silica nanoparticles was satisfactory. The lincomycin-imprinted silica nanoparticles could still be reused after seven adsorption–desorption cycles, which indicated high chemical stability. In addition, the recoveries of the proposed method for lincomycin at three spiked levels of analysis in milk and chicken were 93.3–103.3% and 90.0–100.0%, respectively.

Conclusion: The prepared lincomycin-imprinted silica nanoparticles are feasible for the recognition of target lincomycin with low concentrations in real food samples such as milk and chicken. Our approach makes sample pre-preparation simple, fast, selective, and efficient.

KEYWORDS

boronate affinity, lincomycin, template-immobilized surface imprinting, milk, chicken, silica nanoparticles

1. Introduction

Antimicrobial agents are widely used to prevent and treat diseases and promote growth in animal husbandry (Ding et al., 2021; Khafi et al., 2023). However, food safety issue by veterinary drug residues has become a worldwide public health concern. As a lincosamide antibiotic, lincomycin (Lin) is widely used in human and veterinary medicine due to its excellent antibacterial effect (Dasenaki and Thomaidis, 2015; Koike et al., 2021). Meanwhile, Lin is also used in association with other antimicrobial drugs to treat livestock infections caused by *Bacteroides fragilis*, as well as diseases of the respiratory tract in different animal species (Maddaleno et al., 2019). However, it also has an adverse impact on human products and life because of the irrational use of Lin. Antibiotic residues may lead to disturbances in ecological functions and promote the development and distribution of resistant genes, which pose a potential risk to the environment (Bengtsson-Palme and Larsson, 2016; Andrade et al., 2020). Among the most important effects of Lin getting released into the environment are the transfer of Lin-resistant genes (LRGs) and the alteration of the microbial community, such as the impact on food safety and human health due to crop plant uptake (Mehrtens et al., 2021). It affects people's health when they eat foods containing Lin residue, especially the frequent consumption of milk and chicken products containing Lin. The acceptable maximum residual level (MRL) of Lin in milk and chicken was set at 150 and 200 $\mu g\,kg^{-1}$ by the Codex Alimentarius Commission and the European Union, respectively (Du et al., 2019). Therefore, it is important to have in place an efficient way to evaluate the levels of Lin in animal-derived food samples such as milk and chicken.

Thus far, a variety of analytical methods have been used to evaluate Lin in different real samples including GC–MS (Tao et al., 2011), LC–MS (Khadim et al., 2023), LC–MS/MS (Fernandes-Cunha et al., 2015; Maddaleno et al., 2019; Du et al., 2021; Li et al., 2021), and immunoassay (Zhou et al., 2014; Cao et al., 2015). Although these methods have many advantages, especially good sensitivity and accuracy, most of them suffer from several drawbacks, such as costly instruments, complicated sample preparation, long time consumption, and poor storage stability. This compels the need for a simple, fast, and sensitive quantitative method that absorbs Lin in food samples. However, the low content of Lin and high content of complex interfering substances add to the difficulty and challenges in the direct determination of Lin in food samples using UV detection. Therefore, an efficient sample pre-preparation prior to detection becomes very necessary, including separation and enrichment of Lin in food samples.

Molecularly imprinted polymers (MIPs) have been used as efficient solid phase extraction (SPE) adsorbents on account of their high specificity, easy preparation, low cost, and good physicochemical stability (Vlatakis et al., 1993; Li et al., 2015; Hao et al., 2016). To the best of our knowledge, although there are several reports on the preparation of MIPs for Lin to date (Li et al., 2017; Zhang et al., 2019; Dong et al., 2020), the molecular imprinting used in these studies was performed through a one-pot process. In fact, such an imprinting methodology is bulk imprinting in essence because the thickness of the imprinted coating cannot be calibrated to the size of the template, which thereby greatly affects the imprinting effect. To address these issues, the template-immobilized surface imprinting approach (Li et al., 2015; Hao et al., 2016; Zhang et al., 2022) should be used to prepare imprinting coating on the surface of silica because it can be adjusted to the size of the template effectively. This method of surface imprinting offers several advantages, including easy template removal, high binding capacity, and fast mass transfer. Recently, we used boronate affinity-based oriented surface imprinting to prepare chlorogenic acid-imprinted magnetic nanomaterials and catecholamine-imprinted magnetic nanomaterials, which were applied, respectively, for the selective recognition of chlorogenic acid in fruit juices and for trace analysis of catecholamine in human urine (Li et al., 2020; Li P. et al., 2022). However, the binding capacity of the above imprinted magnetic nanomaterials was relatively low. In addition, this kind of template-immobilized surface imprinting has not been used to develop MIPs for Lin for food safety in previous reports. The pesticide residue of Lin is one of the most important food safety concerns. In this study, a novel boronic acid ligand, FFPBA, has been used for the first time as a functional monomer, and its pKa value has also been measured for the first time. Although boronic acid functionalized magnetic nanoparticles (MNP) were developed for highly efficient capture of lincomycin (Zhang et al., 2023), the selective ability of the boronic acid functionalized magnetic nanoparticles for Lin was weak due to the absence of an imprinting site. To improve its selectivity and binding, boronate affinity-based imprinted nanoparticles specific to Lin were prepared.

In the template-immobilized surface imprinting strategy, template immobilization and removal are the key steps. Fortunately, Lin has a cis-diols structure; boronate affinity materials can covalently bind compounds with cis-diol at high pH values, and boronate esters can dissociate at relatively low pH values under mild ambient conditions (Liu et al., 2012; Qu et al., 2012; Li D. et al., 2022). In addition, 3-fluoro-4-formylphenylboronic acid (FFPBA) has been used for the first time as boronic acid ligands to immobilize and imprint Lin. Silica nanoparticles (SiO_2), due to their good biocompatibility, low toxicity, easy post-modification, high yield synthesis, and easy preparation, can be used successfully as solid substrates (He et al., 2010; Lin et al., 2012; Arabi et al., 2016). Therefore, high-density boronic acid ligands can be formed on the surface of SiO_2 by post-modification reactions. Furthermore, the imprinted coating is important for the binding properties of the imprinted materials. The poly (2-anilinoethanol) with a more hydrophilic domain can be used as a good imprinting coating.

In this study, we attempted to prepare novel Lin-imprinted silica nanoparticles (Lin-imprinted SiO_2@APTES@FFPBA) using a boronate affinity-based template-immobilized surface imprinting approach. As depicted in Figure 1, the imprinting process included three steps. First, Lin was immobilized onto FFPBA-functionalized SiO_2 (SiO_2@APTES@FFPBA) through boronate affinity interaction. Then, the 2-anilinoethanol was self-polymerized on the surface of SiO_2@APTES@FFPBA to form an imprinting coating with appropriate thickness. Generally, the thickness of the imprinting coating should be adjusted to 1/3 to 2/3 of the molecular size of the template in one of the three dimensions. Finally, the Lin template was removed by an acidic solution with SDS to form the MIPs with an imprinting cavity containing FFPBA. Because the obtained imprinting coating could cover excessive binding sites, non-specific adsorption could be effectively eliminated. The prepared Lin-imprinted SiO_2@APTES@FFPBA exhibited several significant advantages, such as good specificity, high binding capacity, fast kinetics, and low binding pH toward Lin. In addition, the recoveries of the proposed method for Lin at three spiked levels of analysis in milk and chicken were 95.3–102.7%

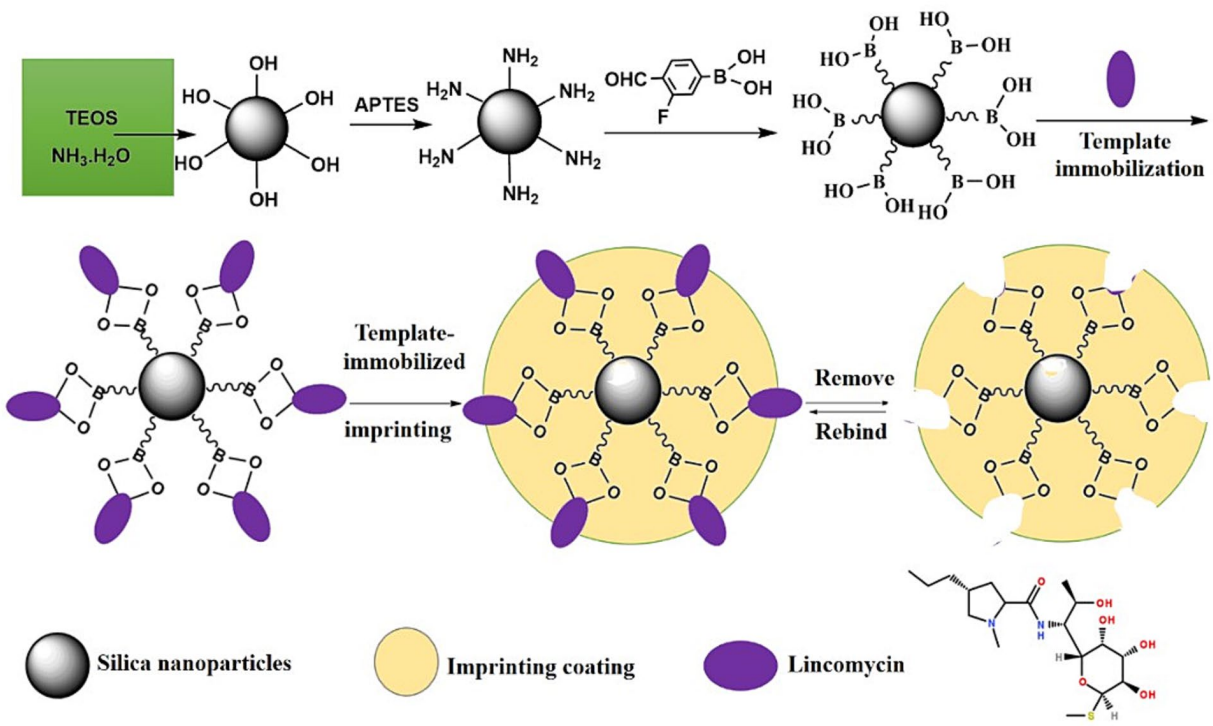

FIGURE 1
The formation mechanism of Lin-imprinted silica nanoparticles by boronate affinity-based template-immobilized surface imprinting.

and 96.8–104.5%, respectively, which indicated the successful detection of Lin in real samples.

2. Experimental materials and methods

2.1. Materials

Adenosine (A), deoxyadenosine (DA), guanosine (G), 2'-O-methylguanosine (Gm), dopamine (Dop), rutin (Rut), quercertin (Que), Baicalein (Bai), Vitamin b12, genistein (Gen), kaempferol (Kae), Lin, desonide (Des), 2-anilinoethanol, tetraethoxysilane (TEOS), (3-amino-propyl) triethoxysilane (APTES), ammonium persulfate (APS), FFPBA, Sodium cyanoborohydride, and anhydrous methanol were purchased from J&K Scientific Ltd. (Shanghai, China). All other reagents were of analytical grade or above and used without further treatment.

2.2. Instruments

Transmission electron microscopy (TEM) characterization was performed on a JEM-1010 system (JEOL, Tokyo, Japan). UV absorbance and the adsorption isotherm measurements were carried out using a U-3010 UV spectrophotometer equipped with a 1-cm cuvette (Kyoto, Japan). The X-ray photoelectron spectroscopy (XPS) was performed with an ESCALAB 250Xi X-ray photoelectron spectrometer (Thermo, USA) with Al Kα radiation (hv = 1486.6 eV). The instrument was calibrated against the C1s band at 284.8 eV. Powder X-ray diffraction (XRD) analyses were carried out using a Bruker D8 Advance diffractometer with Cu Kα radiation, and the scanning angle ranged from 10° to 80° of 2θ.

2.3. Preparation of FFPBA-functionalized silica nanoparticles (SiO_2@APTES@FFPBA)

FFPBA-functionalized MNPs were prepared by the following three-step reaction (Figure 1): (1) synthesis of silica nanoparticles (SiO_2), (2) functionalization with APTES (SiO_2@APTES), and (3) functionalization of SiO_2@APTES using FFPBA by the Schiff base reaction (SiO_2@APTES@FFPBA). The bare SiO_2 was synthesized according to a modified previously reported method (Lin et al., 2014). Briefly, 6 mL of TEOS was gradually added to a mixture of 100 mL ethanol, 4 mL deionized water, and 3.2 mL aqueous solution of 25–28% ammonium. The mixture solutions were vigorously stirred at 30°C for 24 h. The resulting SiO_2 was rinsed with water and ethanol three times in sequence and then vacuum-dried at 40°C overnight. Then, 1.0 mL of APTES was added dropwise to 20 mL anhydrous methanol containing 120 mg SiO_2, and the SiO_2@APTES was obtained by stirring the mixture for 24 h. The resultant SiO_2@APTES was purified by three cycles of centrifugation, separation, and resuspension in ethanol by ultrasonication and dried at room temperature under vacuum for further use. The third step was to functionalize SiO_2@APTES with FFPBA. 100 mg of SiO_2@APTES was added to 150 mL anhydrous methanol containing 2.0 g FFPBA, and the obtained mixture was stirred for 12 h at 30°C. After that, sodium cyanoborohydride was added into the above solution (400 mg every 6 h) and kept for 24 h at 30°C. The

SiO_2@APTES@FFPBA was separated from the mixtures by a magnet and washed with water and ethanol in turn. The dried SiO_2@APTES@FFPBA was obtained using vacuum drying (40°C) and needed cold preservation.

2.4. Selectivity of SiO_2@APTES@FFPBA

The selectivity of SiO_2@APTES@FFPBA was evaluated using A, G, and Lin as cis-diol compounds with DA and Gm as non-cis-diol analogs. The cis-diol or non-cis-diol solution (1 mg/mL) was obtained after they were dissolved in 50 mM PBS (pH 7.0), respectively. SiO_2@APTES@FFPBA of 3 mg were dispersed into 1 mL above solution respectively, and the mixture was shaken at room temperature for 30 min. Then, the obtained targets-treated SiO_2@APTES@FFPBA were collected by magnetic force and rinsed with 500 µL PBS (pH 7.0) three times. After that, the target-treated SiO_2@APTES@FFPBA were eluted with an acetic acid solution for 1 h, and the obtained eluates containing targets were collected.

2.5. Preparation of Lin-imprinted SiO_2@APTES@FFPBA

The Lin-imprinted SiO_2@APTES@FFPBA were prepared according to the boronate affinity-based template-immobilized surface imprinting approach. As depicted in Figure 1, Lin templates were first immobilized onto SiO_2@APTES@FFPBA. Specifically, 100 mg of SiO_2@APTES@FFPBA were dispersed into 20 mL phosphate buffer solution (pH 7.0) containing 20 mg Lin, and the obtained suspension was shaken at 25°C for 1 h. The obtained Lin-immobilized SiO_2@APTES@FFPBA were collected and washed with 50 mM phosphate buffer solution (pH 7.0). Then, 80 mg Lin-immobilized SiO_2@APTES@FFPBA were dispersed into 10 mL 2-anilinoethanol solution (100 mM in pH 7.0 PBS) and shaken at 25°C for 5 min. Subsequently, 10 mL APS solution of 50 mM was added into the above-obtained suspension. The mixture was rapidly sealed and shaken at 25°C for 30 min. The imprinted polymer layer was formed by the self-polymerization of 2-anilinoethanol. Finally, the Lin templates were removed using 100 mM acetic acid and then washed with water and ethanol. The same process was followed for the preparation of non-imprinted SiO_2@APTES@FFPBA, except it did not involve Lin templates.

2.6. Optimization of imprinting conditions

As key imprinting conditions, the concentration of 2-anilinoethanol and polymerization time were investigated by measuring the imprinting effect. The Lin solution of 1 mg/mL in 50 mM phosphate (pH 7.0) was applied as a template solution. An equivalent Lin-imprinted SiO_2@APTES@FFPBA was added to each centrifuge tube. Then, 500 µL of Lin template solution was added to a centrifuge tube with Lin-imprinted SiO_2@APTES@FFPBA and shaken for 1 h at 25°C. After the Lin-immobilized SiO_2@APTES@FFPBA was washed with phosphate buffer of pH 7.0 two to three times, an equivalent 10 mL of 2-anilinoethanol and APS solutions at different concentrations was added in sequence to obtain the concentration of 2-anilinoethanol at 20, 40, 60, 80, and 100 mM. Additionally, the process of polymerization was carried out for a duration of 5–60 min.

The imprinting factor (IF) was calculated by the ratio of Q_{MIPs} to Q_{NIPs}, which was used to evaluate the imprinting effect of Lin-immobilized SiO_2@APTES@FFPBA toward Lin. Q_{MIPs} and Q_{NIPs} (mg/g) represent the adsorption capacities of Lin-immobilized SiO_2@APTES@FFPBA and non-imprinted SiO_2@APTES@FFPBA for Lin.

2.7. Specificity of Lin-imprinted SiO_2@APTES@FFPBA

The specificity of the Lin-immobilized SiO_2@APTES@FFPBA for Lin was evaluated using nine samples, including Lin, Dop, Rut, Que., Bai, VB12, Gen, Des, and Kae. First, an equivalent amount of Lin-imprinted SiO_2@APTES@FFPBA was added to each centrifugal tube of 1.5 mL. Each sample solution (1 mg/mL) of 500 µL was added to each centrifuge tube and shaken at 25°C for 1 h. After being washed with phosphate buffer three times, the Lin-immobilized SiO_2@APTES@FFPBA were eluted using 100 µL of acetic acid solution (pH 2.7) for 2 h. The eluent was measured with UV absorbance at maximum absorption wavelength. The measurement was repeated three times.

2.8. Determination of the pK_a value of FFPBA

The pK_a value of FFPBA was measured according to the previously reported method. UV absorption changes were measured by the titration of 0.1 mM solution of FFPBA in 100 mM phosphate buffer with 1 M sodium hydroxide. The wavelength of the spectrophotometer was set at 268 nm, and a pH meter was fixed in the solution to continuously record the pH of the solution.

2.9. Binding isotherm and Scatchard analysis

The dissociation constant (K_d) and maximum binding capacity (Q_{max}) were determined according to a previously reported method (Li et al., 2015). An equivalent quantity of Lin-immobilized SiO_2@APTES@FFPBA (3 mg each) was mixed with 500 µL of Lin solutions at different concentrations (0.01, 0.02, 0.03, 0.04, 0.05, 0.06, 0.08, 0.10, and 0.12 mg/mL) in centrifuge tubes. Then, the obtained mixture solutions were shaken on a rotator for 1 h at room temperature. The Lin-imprinted SiO_2@APTES@FFPBA were collected, rinsed, and eluted with PBS (pH 7.0) and acetic acid solution, respectively. The obtained eluates were used to measure the Lin in the eluates. The K_d and Q_{max} were calculated based on the following Scatchard equation (Li et al., 2015):

$$\frac{Q_e}{C_s} = \frac{Q_{\max}}{K_d} - \frac{Q_e}{K_d}$$

Q_e and C_s are the binding capacity and the free concentration of the Lin-imprinted SiO_2@APTES@FFPBA for Lin at equilibrium,

respectively. K_d and Qmax can be calculated from the slope and the intercept of the plots of *Qe*/*Cs* versus *Qe*.

2.10. Analysis of Lin in real milk and chicken samples

70 mL of milk was placed in a 100 mL centrifugal tube and shaken with ultrasound for 10 min to achieve a uniform milk sample (Li and Bie, 2017). To determine Lin in milk, 30 mg of Lin-imprinted SiO_2@APTES@FFPBA was added to 15 mL of the milk sample and shaken for 10 min at room temperature. The Lin-imprinted SiO_2@APTES@FFPBA, which absorbed the Lin, was eluted with acetic acid, and the eluent was collected and measured. To evaluate the recoveries of Lin in the milk sample, different amounts of Lin were mixed into milk to obtain milk solutions containing Lin at different concentrations (0.05, 0.15, and 0.30 μg/g). Then, an equivalent quantity of Lin-imprinted SiO_2@APTES@FFPBA was placed in the above-prepared 15 mL milk solution. After washing, Lin-imprinted SiO_2@APTES@FFPBA were eluted with 2 mL acetic acid solution (pH 2.7) each time for three times, and 6 mL of eluent was collected. The feasibility of pretreatment of Lin in milk by Lin-imprinted SiO_2@APTES@FFPBA was analyzed by HPLC-UV.

Chicken samples (20 g) were added to 80 mL acetonitrile and extracted by ultrasonics for 40 min (Li et al., 2017). Then, the extracted solutions were transferred into a 100 mL flask for evaporation and drying on a rotary evaporator. The final residue was dissolved in 20 mL PBS (100 mM in pH 7.0) to form chicken sample solutions containing Lin. Then, 20 mg of Lin-imprinted SiO_2@APTES@FFPBA was added to 5 mL of the chicken sample solutions and shaken for 10 min at room temperature. The Lin-imprinted SiO_2@APTES@FFPBA, which absorbed the Lin, was eluted with acetic acid, and the eluent was collected and measured by absorbance. To evaluate the recoveries of Lin in chicken samples, equivalent amounts of Lin-imprinted SiO_2@APTES@FFPBA were placed in the chicken sample solutions containing Lin at different concentrations (0.10, 0.20, and 0.40 μg/g). Lin-imprinted SiO_2@APTES@FFPBA after adsorption were collected and washed with pH 7.0 PBS. Next, Lin-imprinted SiO_2@APTES@FFPBA were eluted with 2 mL acetic acid solution (pH 2.7) each time for three times, and 6 mL of eluent was collected and analyzed by HPLC-UV.

3. Results and discussion

3.1. Characterization of Lin-imprinted SiO_2@APTES@FFPBA

Figure 2A represents the TEM images of Lin-imprinted SiO_2@APTES@FFPBA. It can be observed clearly that Lin-imprinted SiO_2@APTES@FFPBA exhibits approximately spherical morphologies and relatively narrow size distributions with a diameter of about 100 nm. This result indicated that the Lin-imprinted SiO_2@APTES@FFPBA had satisfactory dispersibility, which is highly advantageous for the selective recognition of Lin.

To verify the successful preparation of Lin-imprinted SiO_2@APTES@FFPBA, X-ray photoelectron survey spectrometry (XPS) of bare SiO_2 and Lin-imprinted SiO_2@APTES@FFPBA was investigated. As shown in Figure 2B, the XPS spectrum exhibited an O 1 s peak at 531 eV and a Si 2p peak at 105 eV in bare SiO_2. While the XPS spectrum exhibited a C 1 s peak at 286 eV, O 1 s peak at 531 eV, Si 2p peak at 105 eV, N 1 s peak at 399 eV, and B 1 s peak at 191 eV in Lin-imprinted SiO_2@APTES@FFPBA. The peak at a binding energy of 191 eV could be assigned to B atoms in the form of Lin-imprinted SiO_2@APTES@FFPBA, which proved successful preparation of Lin-imprinted SiO_2@APTES@FFPBA. In addition, the crystalline nature of bare SiO_2 and Lin-imprinted SiO_2@APTES@FFPBA could be confirmed by XRD analysis. As depicted in Figure 2C, the relatively discernible strong diffraction peaks corresponding to SiO_2 (2θ = 24.2°) were observed in the curves of two samples, which highly corresponded to the crystalline planes of cubic spinel nanostructure of the silica nanoparticles. This result indicated that the structure of the carrier SiO_2 was not changed during the coating process of the imprinted layer.

3.2. Selectivity of SiO_2@FFPBA

The post-modification of SiO_2 with boronic acid is a key for boronate affinity-based template-immobilized surface imprinting. The post-modification of boronic acids can be confirmed by investigating the selectivity of the FFPBA-functionalized SiO_2 for cis-diols. A and G were tested as cis-diol-containing compounds, while DA and Gm were tested as non-cis-diol analogs. As seen in Figure 3, the boronic acid-modified SiO_2 (SiO_2@FFPBA) exhibited a higher binding amount for A or G than DA or Gm under neutral pH conditions (pH 7.0). Obviously, this result indicated that the SiO_2@FFPBA provided excellent selectivity. Because Lin contains one cis-diol, the SiO_2@FFPBA exhibited a relatively high binding capacity for Lin. Clearly, the boronic acid-functionalized SiO_2 exhibited selective binding to cis-diol-containing compounds. These results also confirmed the successful immobilization of boronic acid FFPBA onto the SiO_2.

3.3. Investigation of imprinting conditions

For the boronate affinity-based template-immobilized surface imprinting, the thickness of the imprinted coating on the surface of the SiO_2@FFPBA substrate is key for the binding properties of the imprinted materials. Generally, the thickness of the imprinted coating must be calibrated to a smaller size than the template. As we know, the thickness of the imprinted coating is closely related to the concentration of 2-anilinoethanol and polymerization time, and the influence of these two factors on the imprinting effect was systematically evaluated by IF. The thickness of the imprinting coating on SiO_2 is in direct proportion to the concentration of 2-anilinoethanol. The most appropriate 2-anilinoethanol concentration could be evaluated by the binding capacity of MIP and NIP prepared at different concentrations. As observed from Figure 4A, the most appropriate 2-anilinoethanol concentration was 60 mM, with an IF value reaching 7.11. In addition, the influence of polymerization time on the imprinting effect was also investigated. It can be observed from Figure 4B that the binding capacity of MIP for Lin gradually increased with time from 10 to 30 min, while the NIP gradually decreased. However, when the polymerization time was more than 30 min, the binding capacity of MIP for Lin decreased, and NIP remained nearly

10.3389/fsufs.2023.1271921

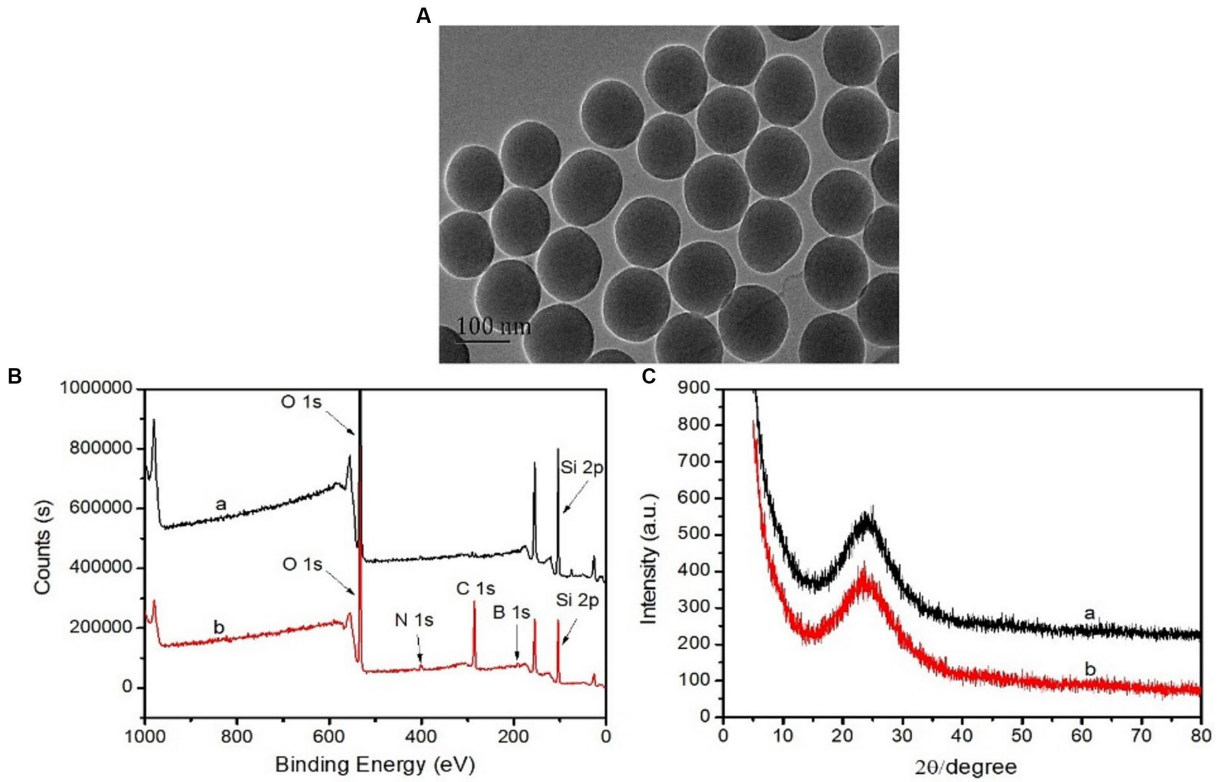

FIGURE 2
TEM images of Lin-imprinted SiO_2@APTES@FFPBA **(A)**, XPS spectra **(B)**, and XRD spectra **(C)** of bare SiO_2 **(A)** and Lin-imprinted SiO_2@APTES@FFPBA **(B)**.

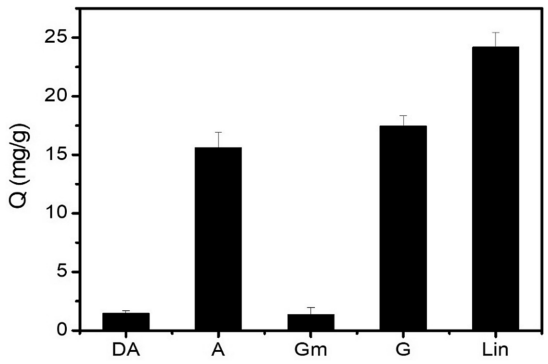

FIGURE 3
The binding amount of different analytes captured by boronic-acid modified SiO_2 (SiO_2@FFPBA). Binding buffer: 50 mM sodium phosphate buffer (pH 7.0); elution solution: 100 mM HAc (pH 2.7); samples: A, DA, Gm, G, and Lin dissolved in binding buffer (1 mg/mL).

constant over time. Clearly, the changing trends of the IF were in good accordance with that of the binding amount of MIP. Thus, the optimal imprinting conditions for Lin was the self-polymerization of 60 mM 2-anilinoethanol for 30 min, which provided the best IF of 7.11. The high IF can be attributed to the fact that there were no boronic acid moieties outside of the imprinted cavities in the current imprinting method. For other antibiotic templates, the good choice is to employ a simple and effective method with the preferred optimized conditions reported here and only tune the polymerization time. If they do not work well, a *de novo* optimization should be carried out.

3.4. Specificity of Lin-imprinted SiO_2@APTES@FFPBA

To evaluate the specificity of Lin-imprinted SiO_2@APTES@FFPBA for Lin, several compounds, including Dop, Rut, Que., Bai, VB12, Gen, Des, and Kae, were selected as competitive compounds. As depicted in Figure 5, compared to the competitive compounds, Lin-imprinted SiO_2@APTES@FFPBA exhibited a higher binding capacity for Lin. In other words, Lin-imprinted SiO_2@APTES@FFPBA provided a higher affinity for Lin. Although Dop, Rut, Bai, and Que. contain cis-diols, Lin-imprinted SiO_2@APTES@FFPBA exhibited a relatively low binding capacity for these compounds. Therefore, the obtained Lin-imprinted SiO_2@APTES@FFPBA possessed excellent specificity toward Lin. This result implied that the boronate affinity-template immobilized surface imprinting strategy gained great success due to the thickness-controllable imprinting coating generated by the in-water self-polymerization of 2-anilinoethanol. Comparatively, the non-imprinted SiO_2@APTES@FFPBA (NIP) only exhibited a very slight affinity toward Lin and other competitive compounds, indicating that the imprinting coating contained only limited non-specific binding sites.

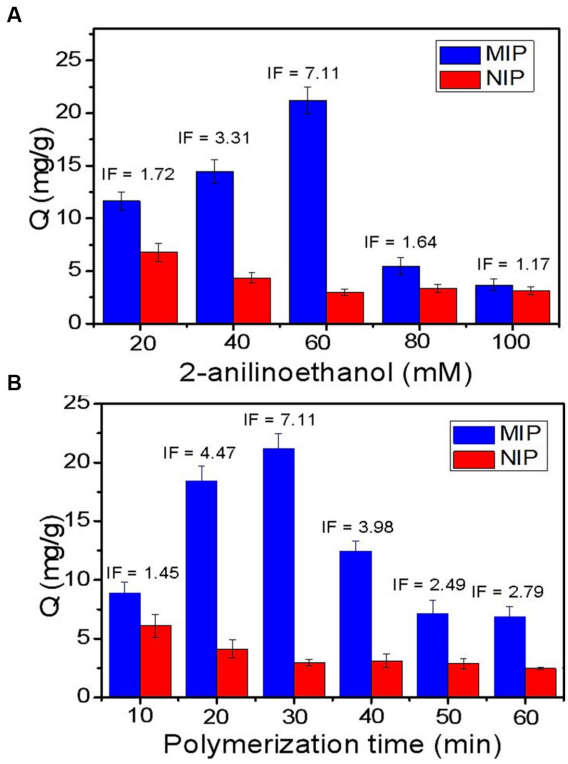

FIGURE 4
Effects of imprinting conditions of the target amount captured by the Lin-imprinted SiO_2@APTES@FFPBA and the imprinting factor (IF). **(A)** concentration of 2-anilinoethanol; **(B)** polymerization time.

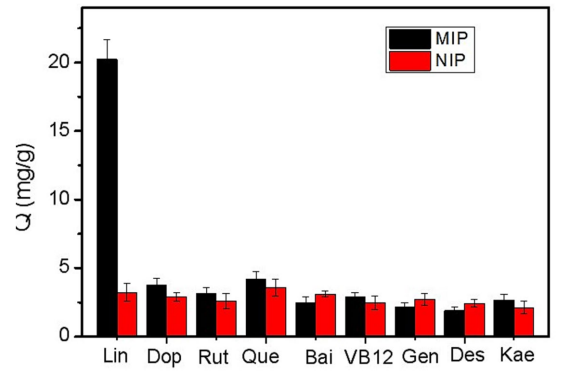

FIGURE 5
Comparison of the amount of different compounds captured by the Lin-imprinted SiO_2@APTES@FFPBA (MIP) and non-imprinted SiO_2@APTES@FFPBA (NIP). Binding buffer: 50 mM phosphate buffer (pH 7.0); eluate: 100 mM HAc (pH 2.7); samples: 1 mg/mL Lin, Dop, Rut, Que., Bai, VB12, Gen, Des, and Kae dissolved in binding buffer.

3.5. Binding pH

The binding pH is an important binding property that is positively related to the binding affinity of boronic acids toward cis-diols. The binding affinity and binding pH are determined by the structures of the boronic acid ligands and supporting materials (Lin-imprinted SiO_2@APTES@FFPBA). As shown in Figure 6A, the pK_a value of FFPBA was measured to be approximately 5.8 due to the presence of electron-withdrawing groups in FFPBA. Clearly, these specific boronic acid ligands could work under low pH conditions of 6.0 (Figure 6B). In addition, the imprinted cavities in the Lin-imprinted SiO_2@APTES@FFPBA could lead to higher binding affinity, thereby providing lower binding pH. To confirm this, the effect of pH on the binding capacity of Lin-imprinted SiO_2@APTES@FFPBA and non-imprinted SiO_2@APTES@FFPBA was investigated. As depicted in Figure 6B, Lin-imprinted SiO_2@APTES@FFPBA exhibited a lower binding pH value (pH 5.0) as compared with SiO_2@APTES@FFPBA (pH 6.0), while non-imprinted MNPs provided very limited binding capacity for Lin. The binding pH shift was due to the imprinted cavities in the structure of Lin-imprinted SiO_2@APTES@FFPBA. Such a pH shift is beneficial because a lower binding pH value generally results from increased affinity toward cis-diol compounds. These results indicated that Lin-imprinted SiO_2@APTES@FFPBA can enlarge the range of pH when directly applied to real samples without requiring pH adjustment.

3.6. Binding equilibrium

In order to evaluate the binding equilibrium time of Lin-imprinted SiO_2@APTES@FFPBA toward Lin, the effect of the response time on binding capacity (Q) was investigated (Figure 7). As seen in Figure 7, Lin-imprinted SiO_2@APTES@FFPBA had a faster adsorption rate than non-imprinted MNPs within the first 6 min. When the response time exceeded 6 min, the adsorption rate quickly slowed down, and the binding reaction reached equilibrium at 6 min. This result implied that most of the binding sites had been occupied by Lin in such a situation. Clearly, such an equilibrium time of Lin-imprinted SiO_2@APTES@FFPBA for Lin was lower than that of other imprinted polymers (8–90 min) (Gu et al., 2010; Li et al., 2012, 2017, 2018a; He et al., 2014; Hao et al., 2016). This result indicated that the Lin-imprinted SiO_2@APTES@FFPBA for Lin showed good binding kinetics.

3.7. Determination of K_d and Q_{max}

As we know, the binding affinity of Lin-imprinted SiO_2@APTES@FFPBA can determine how low concentrations of Lin can be extracted by Lin-imprinted SiO_2@APTES@FFPBA. Therefore, the binding isotherm of the Lin-imprinted SiO_2@APTES@FFPBA toward Lin was investigated to evaluate its binding affinity. As shown in Figure 8A, the Lin-imprinted SiO_2@APTES@FFPBA exhibited much higher binding capacity toward Lin as compared with the non-imprinted SiO_2@APTES@FFPBA. According to the binding isotherm, a Scatchard plot was drawn (Figure 8B), which could provide Q_{max} and K_d values of Lin-imprinted SiO_2@APTES@FFPBA. These were (19.45 ± 1.44) mg/g and (3.65 ± 0.38) × 10^{-5} M, respectively. Clearly, Lin-imprinted SiO_2 exhibited much higher binding capacity than other imprinted nanomaterials (Gu et al., 2010; Li et al., 2018a,b,c,d). Such a high-binding capacity could result from the combination of SiO_2 with easy post-modification and FFPBA with low pK_a. Conversely, it also benefited from the high imprinting efficiency. The strong binding strength of the prepared Lin-imprinted SiO_2@APTES@FFPBA for Lin favors the extraction of Lin of trace concentrations.

10.3389/fsufs.2023.1271921

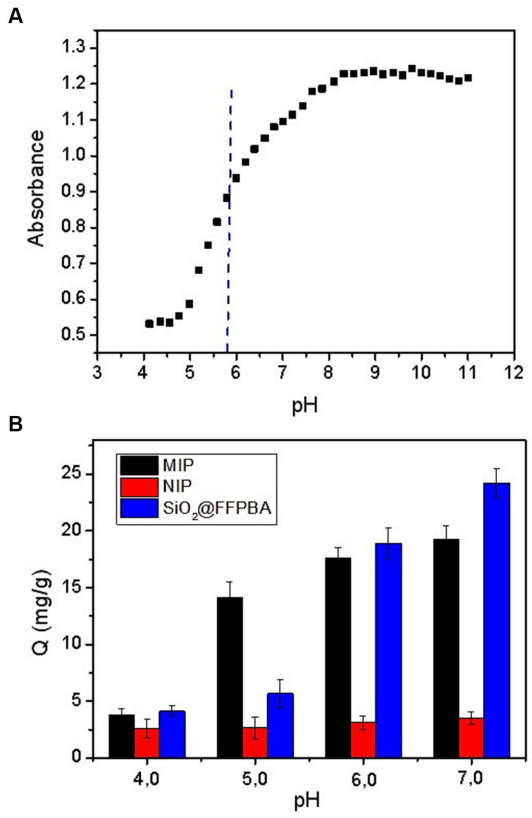

FIGURE 6
(A) The pH-dependence of the absorbance at 268 nm of FFPBA and **(B)** Target binding capability Q of Lin-imprinted SiO_2@APTES@FFPBA (MIP), non-imprinted SiO_2@APTES@FFPBA (NIP), and SiO_2@FFPBA at different pH values. Sample: 1 mg/mL Lin dissolved in 50 mM phosphate buffer (pH 4.0, 5.0, 6.0, and 7.0).

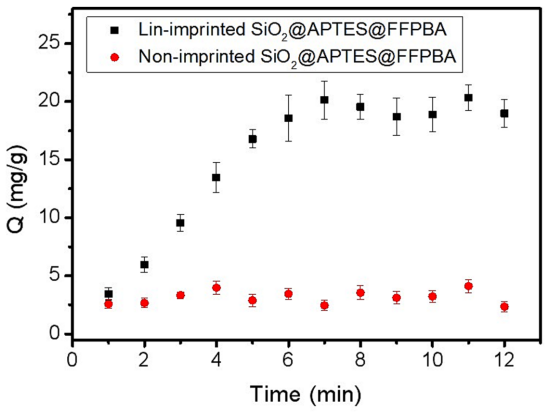

FIGURE 7
Binding equilibrium of Lin-imprinted SiO_2@APTES@FFPBA and non-imprinted SiO_2@APTES@FFPBA. Sample: 1.0 mg/mL of Lin containing 50 mM phosphate, pH 7.0.

3.8. Reproducibility and reusability

The reproducibility of the obtained Lin-imprinted SiO_2@APTES@FFPBA was evaluated by using six batches of Lin-imprinted SiO_2@APTES@FFPBA prepared on different days, and the measurements

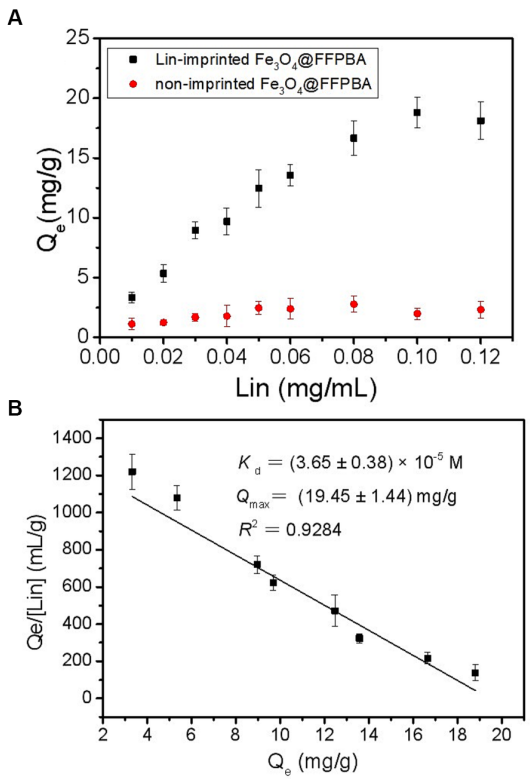

FIGURE 8
(A) Binding isotherms for binding of the Lin-imprinted SiO_2@APTES@FFPBA and non-imprinted SiO_2@APTES@FFPBA to Lin, and **(B)** Scatchard plots for the binding of the Lin-imprinted SiO_2@APTES@FFPBA to Lin.

replicated three times in parallel. It can be observed from Figure 9A that each individually prepared Lin-imprinted SiO_2@APTES@FFPBA exhibited similar binding capacities for Lin (21.30, 18.89, 17.43, 18.16, 17.85, and 17.46) mg/g, respectively. These results indicated that the reproducibility of Lin-imprinted SiO_2@APTES@FFPBA was satisfactory because the boronate affinity-based template immobilized surface imprinting was beneficial.

One of the main advantages of MIPs over native antibodies is their ability to be reused. Thus, the reusability of Lin-imprinted SiO_2@APTES@FFPBA was investigated, and the adsorption–desorption cycle was repeated ten times using the same batch of Lin-imprinted SiO_2@APTES@FFPBA (Figure 9B). Even after six adsorption–desorption cycles, the adsorption capacity of Lin-imprinted SiO_2@APTES@FFPBA = changed very little. Clearly, Lin-imprinted SiO_2@APTES@FFPBA could still be reused after seven adsorption–desorption cycles. Thus, Lin-imprinted SiO_2@APTES@FFPBA possesses high chemical stability.

3.9. Determination of Lin in food samples

In order to investigate the performance of the prepared Lin-imprinted SiO_2@APTES@FFPBA in food samples, the selective separation and determination of Lin from milk and chicken samples by Lin-imprinted SiO_2@APTES@FFPBA was carried out. The obtained results are given in Table 1. Clearly, the content of Lin in chicken was evaluated to be 0.025 μg/g, and no Lin was found in the

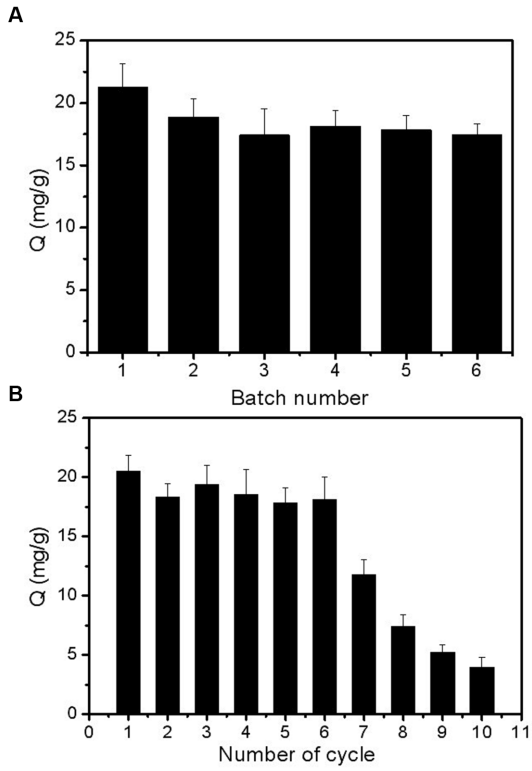

FIGURE 9
Batch-to-batch reproducibility **(A)** and reusability **(B)** of Lin-imprinted SiO_2@APTES@FFPBA. Sample: 1 mg/mL of Lin containing 50 mM phosphate, pH 7.0.

TABLE 1 Results of sample assay and recoveries for the determination of Lin ($n = 3$).

Samples	Spiked levels (μg/g)	Found (μg/g)	Recoveries (%)	RSD (%)
Milk	0.00	Not detected	--	--
	0.05	0.05	100.0	2.5
	0.15	0.14	93.3	4.6
	0.30	0.31	103.3	5.3
Chicken	0.00	0.03	--	5.5
	0.10	0.12	90.0	3.0
	0.20	0.23	100.0	3.7
	0.40	0.41	95.0	4.5

milk solution. In addition, to investigate the accuracy of the method by selective separation and determination of Lin in real food samples, the evaluation of Lin in milk and chicken was performed. The recoveries were investigated with three standard amounts of Lin added in milk and chicken solutions, and the spiked concentration was fixed at 0.05, 0.15, 0.30 μg/mL, and 0.10, 0.20, 0.40 μg/mL, respectively. By extraction and determination of Lin, the recoveries for milk and chicken solutions were shown in Table 1. The recoveries of Lin for milk and chicken solution were evaluated to be 93.3–103.3% and 90.0–100.0%, respectively. In addition, the RSD for milk and chicken solution ranged from 2.5–5.3% and 3.0–4.5%. The results indicated that the proposed method is accurate, sensitive, and selective for the determination of Lin in animal-derived food samples.

4. Conclusion

In this study, we used boronate affinity-based template-immobilized surface imprinting to prepare the boronate affinity-based Lin-imprinted SiO_2@APTES@FFPBA for the first time. The pKa value of FFPBA was first investigated. The use of boronic acid FFPBA in the MIPs provided several highly attractive features, including high specificity, high binding affinity, and low binding pH. Clearly, the prepared Lin-imprinted SiO_2@APTES@FFPBA are feasible for the recognition of target Lin with low concentrations in real food samples. We foresee rapid development and promising applications of this approach in the future.

Data availability statement

The raw data supporting the conclusions of this article will be made available by the authors, without undue reservation.

Author contributions

YZ: Data curation, Formal analysis, Investigation, Methodology, Writing – original draft. YD: Data curation, Methodology, Writing – original draft. YM: Conceptualization, Formal analysis, Project administration, Writing – review & editing. ZZ: Formal analysis, Validation, Writing – original draft. YW: Formal analysis, Validation, Writing – original draft. DL: Formal analysis, Project administration, Resources, Supervision, Validation, Writing – review & editing. SW: Formal analysis, Project administration, Resources, Supervision, Validation, Writing – review & editing.

Funding

The author(s) declare financial support was received for the research, authorship, and/or publication of this article. We are grateful to the Key Research Projects of Henan Higher Education Institutions (No. 22A150017) and the Applied Science and Technology Research Fund of Luoyang Normal University (No. RP2100001241) for the financial support of this work. This work was funded by the National Natural Science Foundation of China (Grant No. 21904003), the University Scientific Research Project of Anhui Province (2022AH050296), and the Open Project of Anhui Engineering Technology Research Center of Biochemical Pharmaceutical (Bengbu Medical College) (Grant No. 2022SYKFZ02).

Conflict of interest

The authors declare that the research was conducted in the absence of any commercial or financial relationships that could be construed as a potential conflict of interest.

Publisher's note

References

Andrade, L., Kelly, M., Hynds, P., Weatherill, J., Majury, A., and O'Dwyer, J. (2020). Groundwater resources as a global reservoir for antimicrobial-resistant bacteria. *Water Res.* 170:115360. doi: 10.1016/j.watres.2019.115360

Arabi, M., Ghaedi, M., and Ostovan, A. (2016). Development of dummy molecularly imprinted based on functionalized silica nanoparticles for determination of acrylamide in processed food by matrix solid phase dispersion. *Food Chem.* 210, 78–84. doi: 10.1016/j.foodchem.2016.04.080

Bengtsson-Palme, J., and Larsson, D. G. (2016). Concentrations of antibiotics predicted to select for resistant bacteria: proposed limits for environmental regulation. *Environ. Int.* 86, 140–149. doi: 10.1016/j.envint.2015.10.015

Cao, S., Song, S., Liu, L., Kong, N., Kuang, H., and Xu, C. (2015). Comparison of an enzyme-linked immunosorbent assay with an Immunochromatographic assay for detection of Lincomycin in Milk and honey. *Immunol. Investig.* 44, 438–450. doi: 10.3109/08820139.2015.1021354

Dasenaki, M. E., and Thomaidis, N. S. (2015). Multi-residue determination of 115 veterinary drugs and pharmaceutical residues in milk powder, butter, fish tissue and eggs using liquid chromatography-tandem mass spectrometry. *Anal. Chim. Acta* 880, 103–121. doi: 10.1016/j.aca.2015.04.013

Ding, L., Zhao, Y., Li, H., Zhang, Q., Yang, W., Fu, B., et al. (2021). A highly selective ratiometric fluorescent probe for doxycycline based on the sensitization effect of bovine serum albumin. *J. Hazard. Mater.* 416:125759. doi: 10.1016/j.jhazmat.2021.125759

Dong, Z., Lu, J., Wu, Y., Meng, M., Yu, C., Sun, C., et al. (2020). Antifouling molecularly imprinted membranes for pretreatment of milk samples: selective separation and detection of lincomycin. *Food Chem.* 333:127477. doi: 10.1016/j.foodchem.2020.127477

Du, L., Li, G., Gong, W., Zhu, J., Liu, L., Zhu, L., et al. (2021). Establishment and validation of the LC-MS/MS method for the determination of lincomycin in human blood: application to an allergy case in forensic science. *J. Forensic Legal Med.* 77:102094. doi: 10.1016/j.jflm.2020.102094

Du, B., Wen, F., Zhang, Y., Zheng, N., Li, S., Li, F., et al. (2019). Presence of tetracyclines, quinolones, lincomycin and streptomycin in milk. *Food Control* 100, 171–175. doi: 10.1016/j.foodcont.2019.01.005

Fernandes-Cunha, G. M., Gouvea, D. R., de Fulgêncio, G. O., Rezende, C. M., da Silva, G. R., Bretas, J. M., et al. (2015). Development of a method to quantify clindamycin in vitreous humor of rabbits' eyes by UPLC-MS/MS: application to a comparative pharmacokinetic study and in vivo ocular biocompatibility evaluation. *J. Pharm. Biomed. Anal.* 102, 346–352. doi: 10.1016/j.jpba.2014.08.023

Gu, X. H., Xu, R., Yuan, G. L., Lu, H., Gu, B. R., and Xie, H. P. (2010). Preparation of chlorogenic acid surface-imprinted magnetic nanoparticles and their usage in separation of traditional Chinese medicine. *Anal. Chim. Acta* 675, 64–70. doi: 10.1016/j.aca.2010.06.033

Hao, Y., Gao, R., Liu, D., He, G., Tang, Y., and Guo, Z. (2016). A facile and general approach for preparation of glycoprotein-imprinted magnetic nanoparticles with synergistic selectivity. *Talanta* 153, 211–220. doi: 10.1016/j.talanta.2016.03.005

He, H., Fu, G., Wang, Y., Chai, Z., Jiang, Y., and Chen, Z. (2010). Imprinting of protein over silica nanoparticles via surface graft copolymerization using low monomer concentration. *Biosens. Bioelectron.* 26, 760–765. doi: 10.1016/j.bios.2010.06.043

He, H., Xiao, D., He, J., Li, H., He, H., Dai, H., et al. (2014). Preparation of a core-shell magnetic ion-imprinted polymer via a sol-gel process for selective extraction of cu(II) from herbal medicines. *Analyst* 139, 2459–2466. doi: 10.1039/c3an02096g

Khadim, A., Yaseen Jeelani, S. U., Khan, M. N., Kumari, S., Raza, A., Ali, A., et al. (2023). Targeted analysis of veterinary drugs in food samples by developing a high-resolution tandem mass spectral library. *J. Agric. Food Chem.* 71, 12839–12848. doi: 10.1021/acs.jafc.3c03715

Khafi, M., Javadi, A., and Mogaddam, M. R. A. (2023). Combination of three-phase extraction with deep eutectic solvent-based dispersive liquid–liquid microextraction for the extraction of some antibiotics from egg samples prior to HPLC-DAD. *Microchem. J.* 190:108652. doi: 10.1016/j.microc.2023.108652

Koike, H., Kanda, M., Hayashi, H., Matsushima, Y., Nakajima, T., Yoshikawa, S., et al. (2021). Monitoring of residual antibacterial agents in animal and fishery products in Tokyo from 2003 to 2019: application and verification of a screening strategy based on microbiological methods. *Food Addit. Contam. Part B Surveill.* 14, 66–73. doi: 10.1080/19393210.2021.1871973

Li, D., and Bie, Z. (2017). Branched polyethyleneimine-assisted boronic acid-functionalized magnetic nanoparticles for the selective enrichment of trace glycoproteins. *Analyst* 142, 4494–4502. doi: 10.1039/c7an01174a

Li, D., Bie, Z., Wang, F., and Guo, E. (2018a). Efficient synthesis of riboflavin-imprinted magnetic nanoparticles by boronate affinity-based surface imprinting for the selective recognition of riboflavin. *Analyst* 143, 4936–4943. doi: 10.1039/c8an01044g

Li, D., Chen, Y., and Liu, Z. (2015). Boronate affinity materials for separation and molecular recognition: structure, properties and applications. *Chem. Soc. Rev.* 44, 8097–8123. doi: 10.1039/c5cs00013k

Li, S., Liu, C., Yin, G., Zhang, Q., Luo, J., and Wu, N. (2017). Aptamer-molecularly imprinted sensor base on electrogenerated chemiluminescence energy transfer for detection of lincomycin. *Biosens. Bioelectron.* 91, 687–691. doi: 10.1016/j.bios.2017.01.038

Li, P., Pang, J., Xu, S., He, H., Ma, Y., and Liu, Z. (2022). A Glycoform-resolved dual-modal Ratiometric immunoassay improves the diagnostic precision for hepatocellular carcinoma. *Angewandte Chemie* 61:e202113528. doi: 10.1002/anie.202113528

Li, G., Shi, Z., and Li, D. (2020). Efficient synthesis of boronate affinity-based chlorogenic acid-imprinted magnetic nanomaterials for the selective recognition of chlorogenic acid in fruit juices. *New J. Chem.* 44, 11013–11021. doi: 10.1039/d0nj01716g

Li, D., Tang, N., Wang, Y., Zhang, Z., Ding, Y., and Tian, X. (2022). Efficient synthesis of boronate affinity-based catecholamine-imprinted magnetic nanomaterials for trace analysis of catecholamine in human urine. *New J. Chem.* 46, 16618–16626. doi: 10.1039/d2nj02552c

Li, D., Tu, T., and Wu, X. (2018c). Efficient preparation of template immobilization based boronate affinity surface-imprinted silica nanoparticles using poly (4-aminobenzyl alcohol) as an imprinting coating for glycoprotein recognition. *Anal. Methods* 10, 4419–4429. doi: 10.1039/C8AY00632F

Li, D., Tu, T., Yang, M., and Xu, C. (2018b). Efficient preparation of surface imprinted magnetic nanoparticles using poly (2-anilinoethanol) as imprinting coating for the selective recognition of glycoprotein. *Talanta* 184, 316–324. doi: 10.1016/j.talanta.2018.03.012

Li, H., Wang, H., Liu, Y., and Liu, Z. (2012). A benzoboroxole-functionalized monolithic column for the selective enrichment and separation of cis-diol containing biomolecules. *Chem. Commun.* 48, 4115–4117. doi: 10.1039/c2cc30230f

Li, D., Yuan, Q., Yang, W., Yang, M., Li, S., and Tu, T. (2018d). Efficient vitamin B12-imprinted boronate affinity magnetic nanoparticles for the specific capture of vitamin B12. *Anal. Biochem.* 561-562, 18–26. doi: 10.1016/j.ab.2018.09.009

Li, Y., Yue, X., Pan, Z., Liu, Y., Shen, M., Zhai, Y., et al. (2021). Development and validation of an LC-MS/MS method for quantifying nine antimicrobials in human serum and its application to study the exposure of Chinese pregnant women to antimicrobials. *J. Clin. Lab. Anal.* 35:e23658. doi: 10.1002/jcla.23658

Lin, Z., Sun, L., Liu, W., Xia, Z., Yang, H., and Chen, G. (2014). Synthesis of boronic acid-functionalized molecularly imprinted silica nanoparticles for glycoprotein recognition and enrichment. *J. Mater. Chem. B* 2, 637–643. doi: 10.1039/c3tb21520b

Lin, Z., Xia, Z., Zheng, J., Zheng, D., Zhang, L., Yang, H., et al. (2012). Synthesis of uniformly sized molecularly imprinted polymer-coated silica nanoparticles for selective recognition and enrichment of lysozyme. *J. Mater. Chem.* 22, 17914–17922. doi: 10.1039/c2jm32734a

Liu, L., Zhang, Y., Zhang, L., Yan, G., Yao, J., Yang, P., et al. (2012). Highly specific revelation of rat serum glycopeptidome by boronic acid-functionalized mesoporous silica. *Anal. Chim. Acta* 753, 64–72. doi: 10.1016/j.aca.2012.10.002

Maddaleno, A., Pokrant, E., Yanten, F., San Martin, B., and Cornejo, J. (2019). Implementation and validation of an analytical method for Lincomycin determination in feathers and edible tissues of broiler chickens by liquid chromatography tandem mass spectrometry. *J. Anal. Methods Chem.* 2019, 4569707–4569708. doi: 10.1155/2019/4569707

Mehrtens, A., Licha, T., and Burke, V. (2021). Occurrence, effects and behaviour of the antibiotic lincomycin in the agricultural and aquatic environment – A review. *Sci. Total Environ.* 778:146306. doi: 10.1016/j.scitotenv.2021.146306

Qu, Y., Liu, J., Yang, K., Liang, Z., Zhang, L., and Zhang, Y. (2012). Boronic acid functionalized core-shell polymer nanoparticles prepared by distillation precipitation polymerization for glycopeptide enrichment. *Chemistry* 18, 9056–9062. doi: 10.1002/chem.201103514

Tao, Y., Chen, D., Yu, G., Yu, H., Pan, Y., Wang, Y., et al. (2011). Simultaneous determination of lincomycin and spectinomycin residues in animal tissues by gas chromatography-nitrogen phosphorus detection and gas chromatography-mass spectrometry with accelerated solvent extraction. *Food Addit. Contam. Part A Chem. Anal. Control Expo. Risk Assess.* 28, 145–154. doi: 10.1080/19440049.2010.538440

Vlatakis, G., Andersson, L. I., Müller, R., and Mosbach, K. (1993). Drug assay using antibody mimics made by molecular imprinting. *Nature* 361, 645–647. doi: 10.1038/361645a0

Zhang, Y., Li, D., Li, Y., Niu, J., and Yuan, M. (2023). Branched polyethylenimine-assisted boronic acid functionalized magnetic nanoparticles for highly efficient capture of lincomycin and clindamycin. *Anal. Methods* 15:2657:2664. doi: 10.1039/d3ay00552f

Zhang, Y., Lu, Y., Zhong, J., Li, W., Wei, Q., and Wang, K. (2019). Molecularly imprinted polymer microspheres prepared via the two-step swelling polymerization for the separation of lincomycin. *J. Appl. Polym. Sci.* 136:47938. doi: 10.1002/app.47938

Zhang, Y., Tian, X., Zhang, Z., Tang, N., Ding, Y., Wang, Y., et al. (2022). Boronate affinity-based template-immobilization surface imprinted quantum dots as fluorescent nanosensors for selective and sensitive detection of myricetin. *Spectrochim. Acta A Mol. Biomol. Spectrosc.* 272:121023. doi: 10.1016/j.saa.2022.121023

Zhou, J., Zhu, K., Xu, F., Wang, W., Jiang, H., Wang, Z., et al. (2014). Development of a microsphere-based fluorescence immunochromatographic assay for monitoring lincomycin in milk, honey, beef, and swine urine. *J. Agric. Food Chem.* 62, 12061–12066. doi: 10.1021/jf5029416